IEEE Access
Multidisciplinary ⋮ Rapid Review ⋮ Open Access Journal

Date of publication xxxx 00, 0000, date of current version xxxx 00, 0000.

Digital Object Identifier 10.1109/ACCESS.2021.DOI

VLF Near-Field Excited by an Arbitrarily Oriented Electric Dipole in a Magnetized Plasma

TONG HE[1], (Member, IEEE), HUI RAN ZENG[2], (Graduate Student Member, IEEE), and KAI LI[2]

[1]Research Center for Intelligent Networks, Zhejiang Laboratory, Hangzhou, Zhejiang 311121 China
[2]College of Information Science and Electronic Engineering, Zhejiang University, Hangzhou, Zhejiang 310027 China

Corresponding author: Kai Li (e-mail: kaili@zju.edu.cn).

This work was supported in part by the National Science Foundation of China under Grant 62001424 and 61571389.

ABSTRACT Since the orientation of a very low frequency (VLF: 3–30 kHz) space-borne antenna relative to the geomagnetic field will change with the satellite orbiting around the earth, precisely computing the near-field excited by an arbitrarily oriented radiator in the ionosphere is of great importance to the antenna analysis in realistic VLF space-borne applications. In this paper, we propose a semi-analytical method for evaluating the near-field of a VLF electric dipole of arbitrary orientation in a magnetized plasma, where the arbitrarily oriented dipole is modeled as the superposition of dipoles parallel and perpendicular to the magnetic field. The near-field in this case consists of the contributions of both the ordinary wave (O-wave) and the extraordinary wave (E-wave). Due to its large attenuation rate, the integral for the O-wave can be directly estimated through numerical integration, while the integral for the E-wave is evaluated with the help of speed-up convergence algorithm and the complex variable theory. Computations show that the O-wave still has comparable amplitudes with the E-wave in the near zone, and the field generated by the dipole perpendicular to the magnetic field is of dominant effects. Moreover, it is found that there exists remarkable "aggregation effect" in the radiation pattern of the E-wave, indicating that the propagable mode in the magnetized plasma propagates mainly along the direction of the magnetic field.

INDEX TERMS Arbitrarily oriented electric dipole, magnetized plasma, near-field, very low frequency electromagnetic wave

I. INTRODUCTION

AS important and valuable devices in information transmission systems, antennas have been extensively studied during the past few decades [1]–[4]. It is known that very low frequency (VLF: 3–30 kHz) is a feasible frequency band for submerged communications and navigation. However, most of the existing VLF transmitting systems were built on massive ground-based stations, which not only required enormous investments but also were difficult to repair in short time once damaged. Fortunately, with the advent of space age, transmitting electromagnetic signals from near-earth satellites were envisioned for submerged communications. But it was only until recent decades, thanks to the rapid development of space technology, VLF space-borne transmitting and propagation experiments became practical. The prevalence of VLF space-borne transmission benefits from the following two aspects. On one hand, since the relative refractive index of the ionosphere is much larger than that of the free space in the VLF band [5], the electrical length of a radiator of same geometric size and its radiation efficiency can be greatly improved in the ionospheric environment. On the other hand, because the onboard radiator will orbit around the earth with the satellite, the propagation distance between the transceivers is shortened remarkably, allowing global communications to be covered with lower power.

In the past few decades, many countries especially including the U.S. and Russia had been attempting to explore the feasibility of transmitting VLF electromagnetic waves from low earth orbit (LEO) satellites and have achieved some progresses. Currently, antennas for VLF transmissions can be divided into two categories, i.e. long and thin linear antennas (such as those used by the National Aeronautics and

This article has been accepted for publication in a future issue of this journal, but has not been fully edited. Content may change prior to final publication. Citation information: DOI 10.1109/ACCESS.2021.3083743, IEEE Access

Space Administration (NASA) and the Italian Space Agency (ASI) [6], [7]) and large loop antennas (such as those used by Russia [8], [9]). Similar applications within the last two decades also include NASA's imager for magnetopause-to-aurora global exploration (IMAGE) project [10], the young engineers 2 satellite (YES-2) launched by the European Space Agency (ESA) [11], and the demonstration and science experiment (DSX) mission conducted by the Air Force Research Laboratory (AFRL) [12]. In the 2017's proposal of developing a VLF transmitter for LEO satellites called the probing of plasmasphere and radiation belts (POPRAD) by Lichtenberger et al. [13], both linear and loop antenna configurations were thought to emit very-long waves propagating along the magnetic field lines and sufficient to reach the other hemisphere. In February 2018, China also put its Zhangheng-1 satellite into orbit for the purpose of measuring VLF electromagnetic fields and plasma parameters [14].

For realistic VLF transmit antennas, current distribution and input impedance are two most critical concerns for researchers as they determine the radiation efficiency of the antenna to a large extent. However, the current distribution and input impedance of an antenna are mainly affected by the near-zone field it radiates, thus accurately calculating the near-field generated by VLF sources in the ionospheric environment becomes the crucial basis for the study of satellite-borne antennas. In the history of investigating radiation field in plasma media, Felsen [15] took the lead in calculation of the field excited by an electric dipole in infinite homogeneous anisotropic media with the well-known "saddle point method". Nevertheless, this method is not applicable in the VLF range since the "saddle point" can not be found in most cases. Subsequently, some interesting works relating to the VLF radiation patterns of arbitrarily oriented electric and magnetic dipoles in a cold magnetoplasma were carried out by Wang and Bell [16]. In 2003, the theory of dipole antenna radiation in the VLF band was investigated by James [17] using the data from rocket experiment "observations of electric-field distributions in the ionospheric plasma: a unique strategy C (OEDIPUS-C)". In 2008, the near-field characteristics of VLF electric dipole antennas in the magnetosphere were systematically examined by the scholar of Stanford University [18], where closed-form solutions for the near-field were obtained via numerical techniques. In a more recent paper by He et al. [19], a semi-analytical method was proposed for evaluating the near-zone field excited by a VLF electric dipole parallel to the geomagnetic field in the ionospheric plasma.

Due to the effects of the earth's magnetic field, the ionosphere will behave remarkable anisotropic properties in the VLF range. Under anisotropic conditions, there coexist two types of waves in the ionospheric plasma, namely, the ordinary wave (O-wave) and the extraordinary wave (E-wave), where the O-wave is an evanescent wave with larger attenuation rate, and the E-wave is a propagable mode with relatively small attenuation. It is known that the problem of far-field radiated by a VLF dipole in an anisotropic medium has been well solved and approximate analytical solutions can be given [20], [21]. Nonetheless, the evaluation of VLF near-field has long been a difficult issue that not many works have thoroughly addressed before. This is because in the VLF range the integrand of the field integral will turn to a highly oscillatory function when the observation point moves to the near region ($k\rho \ll 1$), making accurate estimation of the near-field a challenging task. Moveover, in a real-world VLF space-borne transmitting system, the angle between the radiator and the geomagnetic field is not fixed, but may vary with the motion of the satellite orbiting around the earth [22], [23]. It is regrettable to see that the works mentioned above only tackled the field distribution in isotropic cases or in the far region, and the effect of geomagnetic inclination angle on the radiator was seldom taken into consideration. Despite a feasible method has been proposed to compute the near-field in our previous work [19], the formulations only considered the most basic case (i.e. the dipole is aligned with the magnetic field), and the situation that the radiator may be at arbitrary orientations to the earth's magnetic field due to the movement of the satellite, is still missing. Therefore, in order to further compute the near-field of an arbitrarily oriented antenna in the ionosphere and to provide theoretical support for realistic VLF space-borne transmitting systems, it is necessary to revisit this issue more comprehensively and seek possible solutions.

In this paper, by extending our previous work to a more general case, we will attempt to propose a theoretical method for evaluating the VLF near-field excited by an arbitrarily oriented electric dipole in a magnetized plasma. This method is particularly applicable to cold plasma environments where the sheath effects and wave-particle interactions are neglected. The focus of this paper lies on the investigation of the wave-field structure in the near-zone using both analytical and numerical techniques, with the aim of improving the convergence and accuracy of the integration results when the effect of geomagnetic inclination angle is taken into account. The rest of the paper is organized as follows: the analytical formulations of the problem are given in Sec. II in detail. Based on the proposed method, computations and discussions for various conditions are provided in Sec. III. The paper concludes in Sec. IV.

II. FORMULATIONS OF THE PROBLEM

A. VLF FIELD EXCITED BY AN ARBITRARILY ORIENTED ELECTRIC DIPOLE

Under the effects of the geomagnetic field, the dielectric permittivity of the ionosphere transforms to a 3×3 matrix in the VLF range. Assume the magnetic field is aligned with the z axis and use a cold plasma treatment, the relative dielectric tensor of the ionosphere can be expressed as following based on the classical magnetoionic theory [24], [25]:

$$\tilde{\varepsilon} = \begin{bmatrix} \varepsilon_1 & -i\varepsilon_2 & 0 \\ i\varepsilon_2 & \varepsilon_1 & 0 \\ 0 & 0 & \varepsilon_3 \end{bmatrix} \tag{1}$$

where

$$\varepsilon_1 = 1-\frac{XU}{(U^2-Y^2)},\ \varepsilon_2 = \frac{XY}{(U^2-Y^2)},\ \varepsilon_3 = 1-\frac{X}{U} \quad (2)$$

$$U = 1+i\frac{\nu}{\omega}, \qquad X = \frac{\omega_p^2}{\omega^2}, \qquad Y = \frac{\omega_c}{\omega} \quad (3)$$

$$\omega_p^2 = \frac{Ne^2}{\varepsilon_0 m_e}, \qquad \omega_c = \left|\frac{eB_0}{m_e}\right| \quad (4)$$

In above formulas, ω, ω_p, and ω_c are the operating angular frequency, plasma frequency, and cyclotron frequency, respectively, where B_0 denotes the strength of the geomagnetic field, m_e, e represent the mass and charge quantity of an electron, and N, ν identify the electron density and collision frequency of the ionosphere. Besides, ε_0, μ_0 are the permittivity and permeability of the free space, respectively. In the whole text, a time harmonic factor $\exp(-i\omega t)$ is assumed and applied.

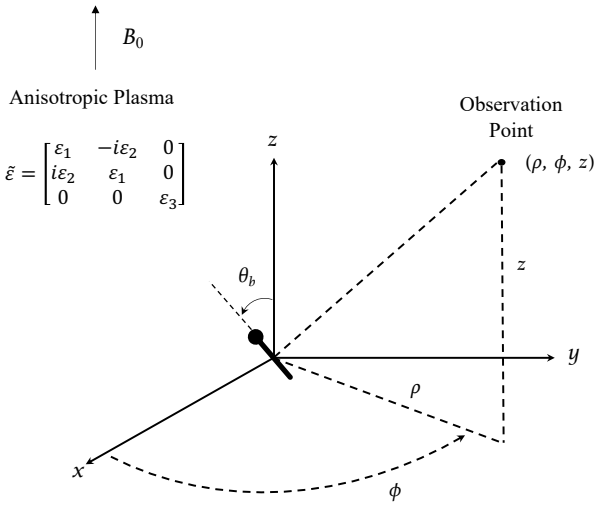

FIGURE 1: Geometry and notations of an arbitrarily oriented electric dipole immersed in a magnetized plasma.

The radiator is assumed to be located in the F_2 layer of the ionosphere, where the electron density is relatively stable [26]. Then the ambient medium of the radiator can be seen as an infinite homogeneous plasma since the wavelength is greatly reduced due to the large refractive index of the ionosphere in the VLF range. The corresponding geometry and notations are illustrated in Fig. 1, where an electric dipole of arbitrary orientation relative to the geomagnetic field is immersed in the magnetized plasma and located at the origin of the coordinate system. For mathematical simplification, we let the arbitrarily oriented dipole always be in the x-z plane by rotating the coordinate axes, and define the dip angle between the dipole and the geomagnetic field as θ_b.

With the help of 3-dimensional Fourier transform, the field radiated by an electric dipole with current moment $Idl = 1$ in a magnetized plasma can be expressed with a triple integral [21]. This integral has the following form in cylindrical coordinates:

$$\boldsymbol{E}(\rho,\varphi,z) = \frac{-i\omega\mu_0}{(2\pi)^3}\int_{-\infty}^{\infty} dk_z \int_0^{2\pi} d\varphi_k \int_0^{\infty} \frac{\boldsymbol{F}(k_z,\lambda,\varphi_k)}{B(k_z,\lambda)} \times \exp\left\{-i\left[k_z z + \lambda\rho\cos\left(\varphi-\varphi_k\right)\right]\right\}\lambda d\lambda \quad (5)$$

where k_z and λ represent the longitudinal and radial components of the wave number, respectively, and φ_k denotes the azimuth angle of the wave number. We have

$$B(k_z,\lambda) = k_0^6\left[\left(\frac{k_z}{k_0}\right)^4\varepsilon_3 + \left(\frac{\lambda}{k_0}\right)^2\left(\varepsilon_2^2-\varepsilon_1^2-\varepsilon_1\varepsilon_3\right) + \left(\frac{k_z}{k_0}\right)^2\left(\frac{\lambda}{k_0}\right)^2(\varepsilon_1+\varepsilon_3) - 2\left(\frac{k_z}{k_0}\right)^2\varepsilon_1\varepsilon_3 + \varepsilon_3\left(\varepsilon_1^2-\varepsilon_2^2\right) + \left(\frac{\lambda}{k_0}\right)^4\varepsilon_1\right] \quad (6)$$

Note that $\boldsymbol{F}$ is a function relating to the orientation of the dipole. When the dipole is aligned with the z axis, i.e. parallel to the magnetic field, the components of $\boldsymbol{F}^z$ are expressed as

$$F_x^z = k_z\lambda(k_z^2+\lambda^2-k_0^2\varepsilon_1)\cos\varphi_k - ik_z\lambda k_0^2\varepsilon_2\sin\varphi_k \quad (7)$$

$$F_y^z = k_z\lambda(k_z^2+\lambda^2-k_0^2\varepsilon_1)\sin\varphi_k + ik_z\lambda k_0^2\varepsilon_2\cos\varphi_k \quad (8)$$

$$F_z^z = (k_z^2+\lambda^2)k_z^2 - k_0^2\varepsilon_1(2k_z^2+\lambda^2) + k_0^4(\varepsilon_1^2-\varepsilon_2^2) \quad (9)$$

If the dipole is oriented along the x axis, i.e. perpendicular to the magnetic field, the three components of $\boldsymbol{F}^x$ are

$$F_x^x = k_0^2(k_0^2\varepsilon_1\varepsilon_3-\varepsilon_1\lambda^2-\varepsilon_3k_z^2)+\lambda^2(k_z^2+\lambda^2-k_0^2\varepsilon_3)\cos^2\varphi_k \quad (10)$$

$$F_y^x = -ik_0^2\varepsilon_2(k_0^2\varepsilon_3+\lambda^2)-\lambda^2(k_z^2+\lambda^2-k_0^2\varepsilon_3)\sin\varphi_k\cos\varphi_k \quad (11)$$

$$F_z^x = k_z\lambda(k_z^2+\lambda^2-k_0^2\varepsilon_1)\cos\varphi_k + ik_z\lambda k_0^2\varepsilon_2\sin\varphi_k \quad (12)$$

A dipole with arbitrary orientation to the background magnetic field can be seen as a superposition of the above two cases. Thus, the components of the corresponding $\boldsymbol{F}^{arbi}$ of an arbitrarily oriented electric dipole as a function of θ_b can be written by

$$\begin{bmatrix} F_x^{arbi} \\ F_y^{arbi} \\ F_z^{arbi} \end{bmatrix} = \begin{bmatrix} F_x^z \\ F_y^z \\ F_z^z \end{bmatrix}\cos\theta_b + \begin{bmatrix} F_x^x \\ F_y^x \\ F_z^x \end{bmatrix}\sin\theta_b \quad (13)$$

By substituting (13) into (5), the integral equations for the field components of an arbitrarily oriented electric dipole in a magnetized plasma are obtained.

B. SIMPLIFICATION OF THE INTEGRAL WITH RESPECT TO φ_K

In order to evaluate the field integral in the near zone precisely, we need to make simplifications to the triple integral. It is seen that the integrands for each field component contain

several sinusoid functions of φ_k, thereby the integral with respect to φ_k will be processed first. We let

$$p_1(k_z,\lambda) = k_z\lambda(k_z^2+\lambda^2-k_0^2\varepsilon_1) \tag{14}$$
$$p_2(k_z,\lambda) = ik_0^2\varepsilon_2 k_z\lambda \tag{15}$$
$$p_3(k_z,\lambda) = k_0^2(k_0^2\varepsilon_1\varepsilon_3-\varepsilon_1\lambda^2-\varepsilon_3 k_z^2) \tag{16}$$
$$p_4(k_z,\lambda) = \lambda^2(k_z^2+\lambda^2-k_0^2\varepsilon_3) \tag{17}$$
$$p_5(\lambda) = ik_0^2\varepsilon_2(k_0^2\varepsilon_3+\lambda^2) \tag{18}$$
$$p_6(k_z,\lambda) = (k_z^2+\lambda^2)k_z^2-k_0^2\varepsilon_1(2k_z^2+\lambda^2)+k_0^4(\varepsilon_1^2-\varepsilon_2^2) \tag{19}$$

then the three components of $\boldsymbol{F}^{arbi}$ can be written in the following forms after substitution of (7)-(12) into (13). We have

$$\begin{aligned} F_x^{arbi} &= [p_1(k_z,\lambda)\cos\varphi_k - p_2(k_z,\lambda)\sin\varphi_k]\cos\theta_b \\ &\quad + [p_3(k_z,\lambda)+p_4(k_z,\lambda)\cos^2\varphi_k]\sin\theta_b \end{aligned} \tag{20}$$
$$\begin{aligned} F_y^{arbi} &= [p_1(k_z,\lambda)\sin\varphi_k + p_2(k_z,\lambda)\cos\varphi_k]\cos\theta_b \\ &\quad - [p_5(\lambda)+p_4(k_z,\lambda)\sin\varphi_k\cos\varphi_k]\sin\theta_b \end{aligned} \tag{21}$$
$$\begin{aligned} F_z^{arbi} &= p_6(k_z,\lambda)\cos\theta_b \\ &\quad + [p_1(k_z,\lambda)\cos\varphi_k + p_2(k_z,\lambda)\sin\varphi_k]\sin\theta_b \end{aligned} \tag{22}$$

The integral form of the Bessel function is now borrowed, which is [27]:

$$J_n(\lambda\rho) = \frac{i^{-n}}{2\pi}\int_0^{2\pi}\exp(i\lambda\rho\cos\theta)\exp(in\theta)d\theta \tag{23}$$

By letting $\theta = \varphi-\varphi_k$ and making proper transformations, the following relations can be obtained. We have

$$\int_0^{2\pi}\exp[-i\lambda\rho\cos(\varphi-\varphi_k)]d\varphi_k = 2\pi J_0(\lambda\rho) \tag{24}$$
$$\begin{aligned} &\int_0^{2\pi}\exp[-i\lambda\rho\cos(\varphi-\varphi_k)]\cos\varphi_k d\varphi_k \\ &\qquad = -2\pi i J_1(\lambda\rho)\cos\varphi \end{aligned} \tag{25}$$
$$\begin{aligned} &\int_0^{2\pi}\exp[-i\lambda\rho\cos(\varphi-\varphi_k)]\sin\varphi_k d\varphi_k \\ &\qquad = -2\pi i J_1(\lambda\rho)\sin\varphi \end{aligned} \tag{26}$$
$$\begin{aligned} &\int_0^{2\pi}\exp[-i\lambda\rho\cos(\varphi-\varphi_k)]\cos^2\varphi_k d\varphi_k \\ &\qquad = \pi[J_0(\lambda\rho)-J_2(\lambda\rho)\cos 2\varphi] \end{aligned} \tag{27}$$
$$\begin{aligned} &\int_0^{2\pi}\exp[-i\lambda\rho\cos(\varphi-\varphi_k)]\sin\varphi_k\cos\varphi_k d\varphi_k \\ &\qquad = -\pi J_2(\lambda\rho)\sin 2\varphi \end{aligned} \tag{28}$$

With the help of (24)-(28), all integrals with respect to φ_k can be expressed using Bessel functions J_0, J_1, J_2. We write

$$\begin{aligned} &\int_0^{2\pi} F_x^{arbi}(k_z,\lambda,\varphi_k)\exp[-i\lambda\rho\cos(\varphi-\varphi_k)]d\varphi_k \\ &= 2\pi\Big\{\sin\theta_b[p_3(k_z,\lambda)+\frac{1}{2}p_4(k_z,\lambda)]J_0(\lambda\rho) \\ &\quad - i\cos\theta_b[p_1(k_z,\lambda)\cos\varphi - p_2(k_z,\lambda)\sin\varphi]J_1(\lambda\rho) \\ &\quad - \frac{1}{2}\sin\theta_b p_4(k_z,\lambda)\cos 2\varphi J_2(\lambda\rho)\Big\} \\ &= 2\pi S_x(k_z,\lambda) \end{aligned} \tag{29}$$

$$\begin{aligned} &\int_0^{2\pi} F_y^{arbi}(k_z,\lambda,\varphi_k)\exp[-i\lambda\rho\cos(\varphi-\varphi_k)]d\varphi_k \\ &= 2\pi\Big\{-\sin\theta_b p_5(\lambda)J_0(\lambda\rho) \\ &\quad - i\cos\theta_b[p_1(k_z,\lambda)\sin\varphi + p_2(k_z,\lambda)\cos\varphi]J_1(\lambda\rho) \\ &\quad + \frac{1}{2}\sin\theta_b p_4(k_z,\lambda)\sin 2\varphi J_2(\lambda\rho)\Big\} \\ &= 2\pi S_y(k_z,\lambda) \end{aligned} \tag{30}$$

$$\begin{aligned} &\int_0^{2\pi} F_z^{arbi}(k_z,\lambda,\varphi_k)\exp[-i\lambda\rho\cos(\varphi-\varphi_k)]d\varphi_k \\ &= 2\pi\Big\{\cos\theta_b p_6(k_z,\lambda)J_0(\lambda\rho) \\ &\quad - i\sin\theta_b[p_1(k_z,\lambda)\cos\varphi + p_2(k_z,\lambda)\sin\varphi]J_1(\lambda\rho)\Big\} \\ &= 2\pi S_z(k_z,\lambda) \end{aligned} \tag{31}$$

By substituting (29)-(31) into (5), all integrals with respect to φ_k can be eliminated and the original triple integral for each field component reduces to a double integral. After rearrangements, we have

$$E_j(\rho,\varphi,z) = \frac{-i\omega\mu_0}{(2\pi)^2}\int_{-\infty}^{\infty}\exp(-ik_z z)dk_z\int_0^{\infty}\frac{S_j(k_z,\lambda)}{B(k_z,\lambda)}\lambda d\lambda \tag{32}$$

where $j = x, y, z$.

C. SIMPLIFICATION OF THE INTEGRAL WITH RESPECT TO K_Z

Next, we will simplify the integral with respect to k_z. First of all, we need to normalize k_z, λ, ρ, z by

$$k_z' = k_z/k_0, \quad \lambda' = \lambda/k_0 \tag{33}$$
$$\rho' = k_0\rho, \quad z' = k_0 z \tag{34}$$

where $k_0 = \omega\sqrt{\mu_0\varepsilon_0}$ denotes the wave number in free space.

After the normalization process, the integral expression for each field component is rewritten as

$$\begin{aligned} E_j(\rho',\varphi,z') = &-\frac{ik_0^2\eta}{(2\pi)^2}\int_{-\infty}^{\infty}\exp(-ik_z' z')dk_z' \\ &\cdot\int_0^{\infty}\frac{S_j'(k_z',\lambda')}{B'(k_z',\lambda')}\lambda' d\lambda', \quad j = x,y,z. \end{aligned} \tag{35}$$

This article has been accepted for publication in a future issue of this journal, but has not been fully edited. Content may change prior to final publication. Citation information: DOI 10.1109/ACCESS.2021.3083743, IEEE Access

where $\eta = \sqrt{\mu_0/\varepsilon_0}$ denotes the wave impedance in free space. In addition, the normalized expressions for S'_x, S'_y, S'_z are

$$\begin{aligned} S'_x(k'_z,\lambda') &= \sin\theta_b\left[p'_3(k'_z,\lambda')+\frac{1}{2}p'_4(k'_z,\lambda')\right]J_0(\lambda'\rho') \\ &\quad - i\cos\theta_b[p'_1(k'_z,\lambda')\cos\varphi - p'_2(k'_z,\lambda')\sin\varphi]J_1(\lambda'\rho') \\ &\quad - \frac{1}{2}\sin\theta_b p'_4(k'_z,\lambda')\cos 2\varphi J_2(\lambda'\rho') \end{aligned} \tag{36}$$

$$\begin{aligned} S'_y(k'_z,\lambda') &= -\sin\theta_b p'_5(\lambda')J_0(\lambda'\rho') \\ &\quad - i\cos\theta_b[p'_1(k'_z,\lambda')\sin\varphi + p'_2(k'_z,\lambda')\cos\varphi]J_1(\lambda'\rho') \\ &\quad + \frac{1}{2}\sin\theta_b p'_4(k'_z,\lambda')\sin 2\varphi J_2(\lambda'\rho') \end{aligned} \tag{37}$$

$$\begin{aligned} S'_z(k'_z,\lambda') &= \cos\theta_b p'_6(k'_z,\lambda')J_0(\lambda'\rho') \\ &\quad - i\sin\theta_b[p'_1(k'_z,\lambda')\cos\varphi + p'_2(k'_z,\lambda')\sin\varphi]J_1(\lambda'\rho') \end{aligned} \tag{38}$$

where

$$p'_1(k'_z,\lambda') = k'_z\lambda'(k'^2_z+\lambda'^2-\varepsilon_1) \tag{39}$$
$$p'_2(k'_z,\lambda') = i\varepsilon_2 k'_z\lambda' \tag{40}$$
$$p'_3(k'_z,\lambda') = \varepsilon_1\varepsilon_3 - \varepsilon_1\lambda'^2 - \varepsilon_3 k'^2_z \tag{41}$$
$$p'_4(k'_z,\lambda') = \lambda'^2(k'^2_z+\lambda'^2-\varepsilon_3) \tag{42}$$
$$p'_5(\lambda') = i\varepsilon_2(\varepsilon_3+\lambda'^2) \tag{43}$$
$$p'_6(k'_z,\lambda') = (k'^2_z+\lambda'^2)k'^2_z - \varepsilon_1(2k'^2_z+\lambda'^2)+\varepsilon_1^2-\varepsilon_2^2 \tag{44}$$

and B' is given by

$$\begin{aligned} B'(k'_z,\lambda') = \varepsilon_3\Bigg\{ & k'^4_z + k'^2_z\left[\lambda'^2\left(1+\frac{\varepsilon_1}{\varepsilon_3}\right)-2\varepsilon_1\right] \\ & + \lambda'^4\left(\frac{\varepsilon_1}{\varepsilon_3}\right) + \lambda'^2\left(\frac{\varepsilon_2^2-\varepsilon_1^2}{\varepsilon_3}-\varepsilon_1\right)+\varepsilon_1^2-\varepsilon_2^2\Bigg\} \end{aligned} \tag{45}$$

It is noted that B' can also be written in the following form through factorization. That is

$$B'(k'_z,\lambda') = \varepsilon_3[k'^2_z - k'^2_1(\lambda')][k'^2_z - k'^2_2(\lambda')] \tag{46}$$

where

$$k'^2_1(\lambda') = \frac{-g(\lambda')+\sqrt{g^2(\lambda')-4h(\lambda')}}{2} \tag{47}$$

$$k'^2_2(\lambda') = \frac{-g(\lambda')-\sqrt{g^2(\lambda')-4h(\lambda')}}{2} \tag{48}$$

and

$$g(\lambda') = \lambda'^2\left(1+\frac{\varepsilon_1}{\varepsilon_3}\right)-2\varepsilon_1 \tag{49}$$

$$h(\lambda') = \lambda'^4\left(\frac{\varepsilon_1}{\varepsilon_3}\right)+\lambda'^2\left(\frac{\varepsilon_2^2-\varepsilon_1^2}{\varepsilon_3}-\varepsilon_1\right)+\varepsilon_1^2-\varepsilon_2^2 \tag{50}$$

It is clear that there exist four zeros for B' at $\pm k'_1$ and $\pm k'_2$, which are also the poles of the integrand in (35). By using the residue theorem, the integral with respect to k'_z can be expressed with the sum of residues at each pole and the double integral in (35) is further reduced to the following single integral:

$$\begin{aligned} E_j(\rho',\varphi,z') = \pm\frac{k_0^2\eta}{4\pi\varepsilon_3}\int_0^\infty \Bigg[& \frac{S'_j(k'_1,\lambda')\exp(ik'_1|z'|)}{k'_1(k'^2_1-k'^2_2)} \\ & - \frac{S'_j(k'_2,\lambda')\exp(ik'_2|z'|)}{k'_2(k'^2_1-k'^2_2)}\Bigg]\lambda' d\lambda', \quad j=x,y,z. \end{aligned} \tag{51}$$

where the plus sign in front of the integral stands for $z'<0$, and the minus sign stands for $z'>0$.

D. EVALUATION OF THE NEAR-FIELD COMPONENT

The integral equation for the field component is now a single integral as shown in (51) and is suitable for evaluation of the near-field. Taking E_x component as example, the field integral can be written as

$$E_x(\rho',\varphi,z') = \pm\frac{k_0^2\eta}{4\pi\varepsilon_3}[I_{x1}(\rho',\varphi,z') - I_{x2}(\rho',\varphi,z')] \tag{52}$$

where I_{x1} and I_{x2} represent the integral contributions of the E-wave and O-wave, respectively. We write

$$I_{x1}(\rho',\varphi,z') = \int_0^\infty \frac{S'_x(k'_1,\lambda')\exp(ik'_1|z'|)}{k'_1(k'^2_1-k'^2_2)}\lambda' d\lambda' \tag{53}$$

$$I_{x2}(\rho',\varphi,z') = \int_0^\infty \frac{S'_x(k'_2,\lambda')\exp(ik'_2|z'|)}{k'_2(k'^2_1-k'^2_2)}\lambda' d\lambda' \tag{54}$$

By expanding the expressions of $S'_x(k'_1,\lambda')$ and $S'_x(k'_2,\lambda')$ in above formulas, I_{x1} turns to

$$\begin{aligned} I_{x1}(\rho',\varphi,z') = & \sin\theta_b I^{(1)}_{x1}(\rho',z') - i\cos\theta_b I^{(2)}_{x1}(\rho',\varphi,z') \\ & - \frac{1}{2}\sin\theta_b I^{(3)}_{x1}(\rho',\varphi,z') \end{aligned} \tag{55}$$

where

$$\begin{aligned} I^{(1)}_{x1}(\rho',z') = \int_0^\infty & \frac{[p'_3(k'_1,\lambda')+\frac{1}{2}p'_4(k'_1,\lambda')]}{k'_1(k'^2_1-k'^2_2)} \\ & \cdot\exp(ik'_1|z'|)J_0(\lambda'\rho')\lambda' d\lambda' \end{aligned} \tag{56}$$

$$\begin{aligned} I^{(2)}_{x1}(\rho',\varphi,z') = \int_0^\infty & \frac{[p'_1(k'_1,\lambda')\cos\varphi - p'_2(k'_1,\lambda')\sin\varphi]}{k'_1(k'^2_1-k'^2_2)} \\ & \cdot\exp(ik'_1|z'|)J_1(\lambda'\rho')\lambda' d\lambda' \end{aligned} \tag{57}$$

$$\begin{aligned} I^{(3)}_{x1}(\rho',\varphi,z') = \int_0^\infty & \frac{p'_4(k'_1,\lambda')\cos 2\varphi}{k'_1(k'^2_1-k'^2_2)} \\ & \cdot\exp(ik'_1|z'|)J_2(\lambda'\rho')\lambda' d\lambda' \end{aligned} \tag{58}$$

and I_{x2} becomes

$$\begin{aligned} I_{x2}(\rho',\varphi,z') = & \sin\theta_b I^{(1)}_{x2}(\rho',z') - i\cos\theta_b I^{(2)}_{x2}(\rho',\varphi,z') \\ & - \frac{1}{2}\sin\theta_b I^{(3)}_{x2}(\rho',\varphi,z') \end{aligned} \tag{59}$$

This article has been accepted for publication in a future issue of this journal, but has not been fully edited. Content may change prior to final publication. Citation information: DOI 10.1109/ACCESS.2021.3083743, IEEE Access

where

$$I_{x2}^{(1)}(\rho',z') = \int_0^\infty \frac{\left[p_3'(k_2',\lambda') + \frac{1}{2}p_4'(k_2',\lambda')\right]}{k_2'(k_1'^2 - k_2'^2)} \cdot \exp(ik_2'|z'|)J_0(\lambda'\rho')\lambda' d\lambda' \quad (60)$$

$$I_{x2}^{(2)}(\rho',\varphi,z') = \int_0^\infty \frac{\left[p_1'(k_2',\lambda')\cos\varphi - p_2'(k_2',\lambda')\sin\varphi\right]}{k_2'(k_1'^2 - k_2'^2)} \cdot \exp(ik_2'|z'|)J_1(\lambda'\rho')\lambda' d\lambda' \quad (61)$$

$$I_{x2}^{(3)}(\rho',\varphi,z') = \int_0^\infty \frac{p_4'(k_2',\lambda')\cos 2\varphi}{k_2'(k_1'^2 - k_2'^2)} \cdot \exp(ik_2'|z'|)J_2(\lambda'\rho')\lambda' d\lambda' \quad (62)$$

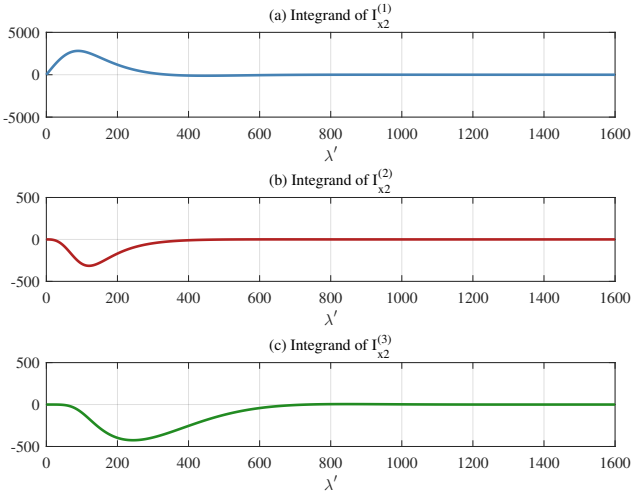

FIGURE 2: Real part of the integrand of (a) $I_{x2}^{(1)}$, (b) $I_{x2}^{(2)}$, (c) $I_{x2}^{(3)}$ versus λ'. ($f = 10$ kHz, $z = \rho = 0.1\lambda_e$, $\varphi = 30°$.)

Since the O-wave is an evanescent wave with great attenuation rate, we first discuss the evaluation of the integral I_{x2}. The integrands of the three integrals corresponding to the contribution of the O-wave are depicted in Fig. 2 with $f = 10$ kHz, $z = \rho = 0.1\lambda_e$ (where λ_e denotes the wavelength of the E-wave along the magnetic field), and $\varphi = 30°$. It is observed from Fig. 2 that all integrands of I_{x2} converge rapidly with λ' due to the larger imaginary part of k_2' [19]. Thus, $I_{x2}^{(1)}$, $I_{x2}^{(2)}$, $I_{x2}^{(3)}$ can be directly evaluated through numerical integration with satisfactory accuracy.

However, due to the small attenuation rate of the E-wave, the integrands of I_{x1} are all oscillating functions when the observation point is in the near region (as can be seen from Fig. 3), indicating that the integrals $I_{x1}^{(1)}$, $I_{x1}^{(2)}$, $I_{x1}^{(3)}$ are not suitable for direct evaluation. Here, we will adopt a speed-up convergence algorithm to pre-process the integrands of $I_{x1}^{(1)}$, $I_{x1}^{(2)}$, and $I_{x1}^{(3)}$. Let $Q(\lambda') = g^2(\lambda') - 4h^2(\lambda')$, when λ' approaches to a very large number, we have

$$\begin{aligned} k_1'^2 - k_2'^2 &= \sqrt{Q(\lambda')} = \sqrt{g^2(\lambda') - 4h(\lambda')} \\ &= \sqrt{\lambda'^4\left(1 - \frac{\varepsilon_1}{\varepsilon_3}\right)^2 - 4\lambda'^2\frac{\varepsilon_2^2}{\varepsilon_3} + 4\varepsilon_2^2} \\ &\approx \lambda'^2\left(1 - \frac{\varepsilon_1}{\varepsilon_3}\right) - \frac{2\varepsilon_2^2}{\varepsilon_3 - \varepsilon_1} = \left(1 - \frac{\varepsilon_1}{\varepsilon_3}\right)(\lambda'^2 - a^2) \end{aligned} \quad (63)$$

where

$$a^2 = \frac{2\varepsilon_2^2\varepsilon_3}{(\varepsilon_1 - \varepsilon_3)^2} \quad (64)$$

Substitute (63) into (47), $k_1'^2$ can be approximated as

$$k_1'^2(\lambda') = \frac{-g(\lambda') + \sqrt{Q(\lambda')}}{2} \approx -\frac{\varepsilon_1}{\varepsilon_3}(\lambda'^2 - b^2) \quad (65)$$

where

$$b^2 = \frac{\varepsilon_2^2\varepsilon_3}{\varepsilon_1(\varepsilon_1 - \varepsilon_3)} + \varepsilon_3 \quad (66)$$

it follows that

$$k_1'(\lambda') \approx \sqrt{-\frac{\varepsilon_1}{\varepsilon_3}}\sqrt{\lambda'^2 - b^2} = k_1^*(\lambda') \quad (67)$$

By utilizing the relations between Bessel functions and Hankel functions, which are

$$J_n(\lambda\rho) = \frac{1}{2}\left[H_n^{(1)}(\lambda\rho) + H_n^{(2)}(\lambda\rho)\right] \quad (68)$$

$$H_n^{(1)}(-\lambda\rho) = -H_n^{(2)}(\lambda\rho) \quad (69)$$

(56)-(58) can be rewritten in the following forms after introducing the speed-up convergence algorithm. We have

$$\begin{aligned} I_{x1}^{(1)}(\rho',z') = &\int_0^\infty \left\{\frac{\left[p_3'(k_1',\lambda') + \frac{1}{2}p_4'(k_1',\lambda')\right]\exp(ik_1'|z'|)}{k_1'(k_1'^2 - k_2'^2)} - f_x^{(1)}(\lambda')\right\}J_0(\lambda'\rho')\lambda' d\lambda' \\ &+ \frac{1}{2}\int_{-\infty}^\infty f_x^{(1)}(\lambda')H_0^{(1)}(\lambda'\rho')\lambda' d\lambda' \\ &= I_{x1}^{(1.1)} + \frac{1}{2}I_{x1}^{(1.2)} \end{aligned} \quad (70)$$

$$\begin{aligned} &I_{x1}^{(2)}(\rho',\varphi,z') = \\ &\int_0^\infty \left\{\frac{\left[p_1'(k_1',\lambda')\cos\varphi - p_2'(k_1',\lambda')\sin\varphi\right]\exp(ik_1'|z'|)}{k_1'(k_1'^2 - k_2'^2)} - f_x^{(2)}(\lambda')\right\}J_1(\lambda'\rho')\lambda' d\lambda' \\ &+ \frac{1}{2}\int_{-\infty}^\infty f_x^{(2)}(\lambda')H_1^{(1)}(\lambda'\rho')\lambda' d\lambda' \\ &= I_{x1}^{(2.1)} + \frac{1}{2}I_{x1}^{(2.2)} \end{aligned} \quad (71)$$

This article has been accepted for publication in a future issue of this journal, but has not been fully edited. Content may change prior to final publication. Citation information: DOI 10.1109/ACCESS.2021.3083743, IEEE Access

$$I_{x1}^{(3)}(\rho',\varphi,z') = \int_0^\infty \left[\frac{p_4'(k_1',\lambda')\cos 2\varphi \exp(ik_1'|z'|)}{k_1'(k_1'^2-k_2'^2)} - f_x^{(3)}(\lambda')\right] J_2(\lambda'\rho')\lambda' d\lambda' + \frac{1}{2}\int_{-\infty}^{\infty} f_x^{(3)}(\lambda') H_2^{(1)}(\lambda'\rho')\lambda' d\lambda' = I_{x1}^{(3.1)} + \frac{1}{2} I_{x1}^{(3.2)} \tag{72}$$

where

$$f_x^{(1)}(\lambda') \approx \frac{\left[p_3'(k_1^*,\lambda') + \frac{1}{2}p_4'(k_1^*,\lambda')\right]\exp(ik_1^*|z'|)}{k_1^*\sqrt{Q(\lambda')}} \tag{73}$$

$$f_x^{(2)}(\lambda') \approx \frac{\left[p_1'(k_1^*,\lambda')\cos\varphi - p_2'(k_1^*,\lambda')\sin\varphi\right]\exp(ik_1^*|z'|)}{k_1^*\sqrt{Q(\lambda')}} \tag{74}$$

$$f_x^{(3)}(\lambda') \approx \frac{p_4'(k_1^*,\lambda')\cos 2\varphi \exp(ik_1^*|z'|)}{k_1^*\sqrt{Q(\lambda')}} \tag{75}$$

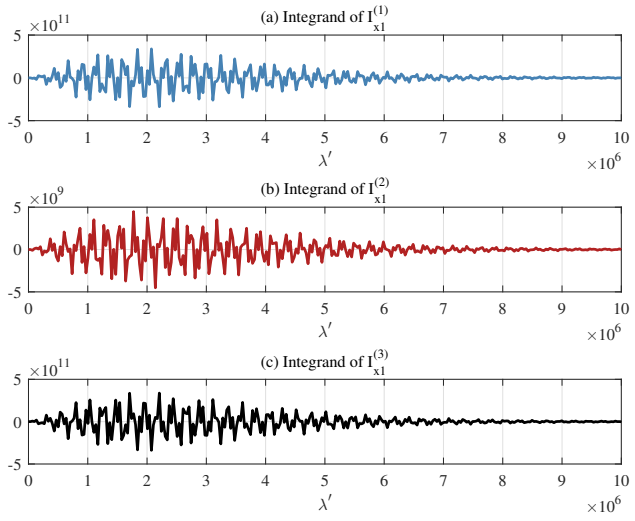

FIGURE 3: Real part of the integrand of (a) $I_{x1}^{(1)}$, (b) $I_{x1}^{(2)}$, (c) $I_{x1}^{(3)}$ versus λ' before applying the speed-up convergence algorithm. ($f = 10$ kHz, $z = \rho = 0.1\lambda_e$, $\varphi = 30°$.)

Pre-processed by the speed-up convergence algorithm, the integrands of the former integrals of (70)-(72) (we denote them as $I_{x1}^{(1.1)}$, $I_{x1}^{(2.1)}$, $I_{x1}^{(3.1)}$) become fast converging functions as well and $I_{x1}^{(1.1)}$, $I_{x1}^{(2.1)}$, $I_{x1}^{(3.1)}$ are now integrable as is shown in Fig. 4. For the latter integrals in (70)-(72) (we denote them as $I_{x1}^{(1.2)}$, $I_{x1}^{(2.2)}$, $I_{x1}^{(3.2)}$), all integrands only possess a pole at $\lambda' = a$ and a branch point at $\lambda' = b$ in the upper plane of λ' (assume the imaginary parts of a and b are positive). Therefore, based on the complex variable theory,

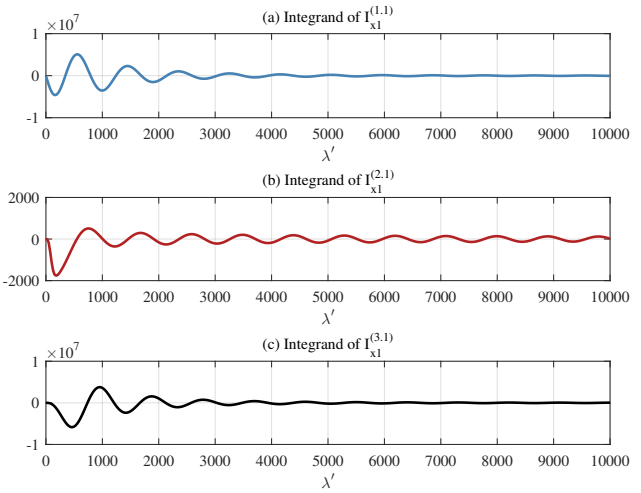

FIGURE 4: Real part of the integrand of (a) $I_{x1}^{(1.1)}$, (b) $I_{x1}^{(2.1)}$, (c) $I_{x1}^{(3.1)}$ versus λ' after applying the speed-up convergence algorithm. ($f = 10$ kHz, $z = \rho = 0.1\lambda_e$, $\varphi = 30°$.)

$I_{x1}^{(1.2)}$, $I_{x1}^{(2.2)}$, and $I_{x1}^{(3.2)}$ can be further expressed as follows:

$$I_{x1}^{(1.2)} = \int_{-\infty}^{\infty} f_x^{(1)}(\lambda') H_0^{(1)}(\lambda'\rho')\lambda' d\lambda' = \pi i H_0^{(1)}(a\rho') \cdot \frac{\left\{p_3'[k_1^*(a),a] + \frac{1}{2}p_4'[k_1^*(a),a]\right\}\exp[ik_1^*(a)|z'|]}{k_1^*(a)\left(1-\frac{\varepsilon_1}{\varepsilon_3}\right)} + \int_\Gamma f_x^{(1)}(\lambda') H_0^{(1)}(\lambda'\rho')\lambda' d\lambda' \tag{76}$$

$$I_{x1}^{(2.2)} = \int_{-\infty}^{\infty} f_x^{(2)}(\lambda') H_1^{(1)}(\lambda'\rho')\lambda' d\lambda' = \pi i H_1^{(1)}(a\rho') \cdot \frac{\left\{p_1'[k_1^*(a),a]\cos\varphi - p_2'[k_1^*(a),a]\sin\varphi\right\}\exp[ik_1^*(a)|z'|]}{k_1^*(a)\left(1-\frac{\varepsilon_1}{\varepsilon_3}\right)} + \int_\Gamma f_x^{(2)}(\lambda') H_1^{(1)}(\lambda'\rho')\lambda' d\lambda' \tag{77}$$

$$I_{x1}^{(3.2)} = \int_{-\infty}^{\infty} f_x^{(3)}(\lambda') H_2^{(1)}(\lambda'\rho')\lambda' d\lambda' = \pi i H_2^{(1)}(a\rho') \cdot \frac{p_4'[k_1^*(a),a]\cos 2\varphi \exp[ik_1^*(a)|z'|]}{k_1^*(a)\left(1-\frac{\varepsilon_1}{\varepsilon_3}\right)} + \int_\Gamma f_x^{(3)}(\lambda') H_2^{(1)}(\lambda'\rho')\lambda' d\lambda' \tag{78}$$

Note that the first terms in (76)-(78) are the residues at the pole $\lambda' = a$, while the second terms represent the integral along the branch line Γ, where Γ is a branch line circling around the branch point $\lambda' = b$. The locations of the pole, branch point, and branch line in the upper complex plane of λ' are illustrated in Fig. 5. If we define $b = \beta + i\gamma$, it is readily verified that $\beta \ll \gamma$, and at the branch point we have $\lambda'\rho' \approx \gamma\rho' \gg 1$ as long as $\rho \geq 0.05\lambda_e$ [19]. In this case, the Hankel functions can be expanded in its asymptotic forms. If

This article has been accepted for publication in a future issue of this journal, but has not been fully edited. Content may change prior to final publication. Citation information: DOI 10.1109/ACCESS.2021.3083743, IEEE Access

we let $\lambda' = b + i\gamma\tau^2$ at the two sides of the branch line, then the Hankel functions can be written as

$$H_0^{(1)}(\lambda'\rho') \approx \sqrt{\frac{2}{\pi\lambda'\rho'}}e^{i(\lambda'\rho'-\frac{\pi}{4})} = \sqrt{\frac{2}{\pi(b+i\gamma\tau^2)\rho'}}e^{i\left(b\rho'-\frac{\pi}{4}\right)}e^{-\gamma\rho'\tau^2} \quad (79)$$

$$H_1^{(1)}(\lambda'\rho') \approx \sqrt{\frac{2}{\pi\lambda'\rho'}}e^{i(\lambda'\rho'-\frac{3\pi}{4})} = \sqrt{\frac{2}{\pi(b+i\gamma\tau^2)\rho'}}e^{i\left(b\rho'-\frac{3\pi}{4}\right)}e^{-\gamma\rho'\tau^2} \quad (80)$$

$$H_2^{(1)}(\lambda'\rho') \approx \sqrt{\frac{2}{\pi\lambda'\rho'}}e^{i(\lambda'\rho'-\frac{5\pi}{4})} = \sqrt{\frac{2}{\pi(b+i\gamma\tau^2)\rho'}}e^{i\left(b\rho'-\frac{5\pi}{4}\right)}e^{-\gamma\rho'\tau^2} \quad (81)$$

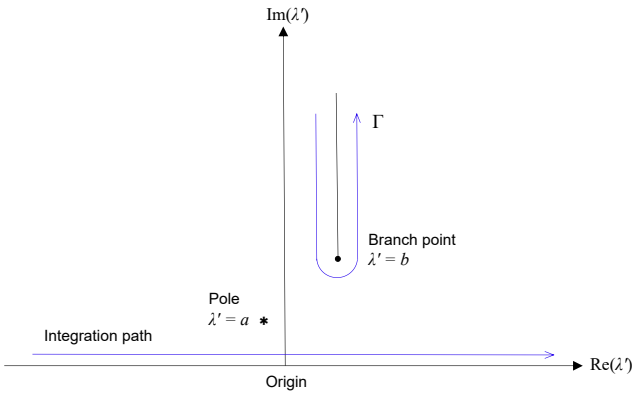

FIGURE 5: Locations of the pole, branch point, and branch line in the upper complex plane of λ'.

Because $\gamma\rho' \gg 1$, it is deduced from the attenuation characteristic of the exponential factor that the main contribution of the integral along the branch line concentrates near the branch point. Hence, we can further approximate k_1^* as

$$k_1^* = \sqrt{-\frac{\varepsilon_1}{\varepsilon_3}}\sqrt{\lambda'^2 - b^2} = \sqrt{-\frac{\varepsilon_1}{\varepsilon_3}}\sqrt{(b+i\gamma\tau^2)^2 - b^2} \approx \sqrt{\frac{2\gamma b\varepsilon_1}{\varepsilon_3}}e^{i\frac{3}{4}\pi}\tau \quad (82)$$

It is noted that the phase of k_1^* has a difference of $180°$ at the two sides of Γ. By substitutions of (79)-(81) and (82) into the second terms of (76)-(78) separately and use approximation $\lambda' \approx b$, all the integrals along the branch line Γ can be rewritten in the following forms:

$$\int_\Gamma f_x^{(1)}(\lambda')H_0^{(1)}(\lambda'\rho')\lambda' d\lambda' = \frac{2i\varepsilon_3^{\frac{3}{2}}\sqrt{\gamma}e^{ib\rho'}}{\sqrt{\pi\rho'\varepsilon_1}(\varepsilon_1-\varepsilon_3)(b^2-a^2)} \cdot \int_{-\infty}^{\infty}(c_{x1}\tau^2 + c_{x2})e^{i\sqrt{\frac{-2i\gamma b\varepsilon_1}{\varepsilon_3}}\tau|z'|}e^{-\gamma\rho'\tau^2}d\tau \quad (83)$$

$$\int_\Gamma f_x^{(2)}(\lambda')H_1^{(1)}(\lambda'\rho')\lambda' d\lambda' = \frac{2\varepsilon_3^{\frac{3}{2}}\sqrt{\gamma}e^{ib\rho'}}{\sqrt{\pi\rho'\varepsilon_1}(\varepsilon_1-\varepsilon_3)(b^2-a^2)} \cdot \int_{-\infty}^{\infty}(c_{x3}\tau^3 + c_{x4}\tau)e^{i\sqrt{\frac{-2i\gamma b\varepsilon_1}{\varepsilon_3}}\tau|z'|}e^{-\gamma\rho'\tau^2}d\tau \quad (84)$$

$$\int_\Gamma f_x^{(3)}(\lambda')H_2^{(1)}(\lambda'\rho')\lambda' d\lambda' = \frac{-2i\varepsilon_3^{\frac{3}{2}}\sqrt{\gamma}e^{ib\rho'}}{\sqrt{\pi\rho'\varepsilon_1}(\varepsilon_1-\varepsilon_3)(b^2-a^2)} \cdot \int_{-\infty}^{\infty}(c_{x5}\tau^2 + c_{x6})e^{i\sqrt{\frac{-2i\gamma b\varepsilon_1}{\varepsilon_3}}\tau|z'|}e^{-\gamma\rho'\tau^2}d\tau \quad (85)$$

where

$$c_{x1} = i\varepsilon_1 b\gamma\left(2 - \frac{b^2}{\varepsilon_3}\right) \quad (86)$$

$$c_{x2} = \varepsilon_1\varepsilon_3 - \varepsilon_1 b^2 + \frac{1}{2}b^2(b^2-\varepsilon_3) \quad (87)$$

$$c_{x3} = \left(\frac{-2i\gamma b\varepsilon_1}{\varepsilon_3}\right)^{\frac{3}{2}} b\cos\varphi \quad (88)$$

$$c_{x4} = \sqrt{\frac{-2i\gamma b\varepsilon_1}{\varepsilon_3}}b\left[(b-\varepsilon_1)\cos\varphi - i\varepsilon_2\sin\varphi\right] \quad (89)$$

$$c_{x5} = \frac{-2i\gamma b^3\varepsilon_1}{\varepsilon_3}\cos 2\varphi \quad (90)$$

$$c_{x6} = b^2(b^2-\varepsilon_3)\cos 2\varphi \quad (91)$$

If we define

$$W_1(\rho', z') = \int_{-\infty}^{\infty}\tau^4 e^{-u\tau^2}e^{q\tau}d\tau \quad (92)$$

$$W_2(\rho', z') = \int_{-\infty}^{\infty}\tau^2 e^{-u\tau^2}e^{q\tau}d\tau \quad (93)$$

$$W_3(\rho', z') = \int_{-\infty}^{\infty}e^{-u\tau^2}e^{q\tau}d\tau \quad (94)$$

$$W_4(\rho', z') = \int_{-\infty}^{\infty}\tau^3 e^{-u\tau^2}e^{q\tau}d\tau \quad (95)$$

$$W_5(\rho', z') = \int_{-\infty}^{\infty}\tau e^{-u\tau^2}e^{q\tau}d\tau \quad (96)$$

by utilizing the integral equation of exponential functions [27]

$$\int_{-\infty}^{\infty}e^{-ux^2\pm qx}dx = \sqrt{\frac{\pi}{u}}e^{\frac{q^2}{4u}}, \quad Re(u) > 0. \quad (97)$$

and let

$$u = \gamma\rho', \qquad q = i\sqrt{\frac{-2i\gamma b\varepsilon_1}{\varepsilon_3}}|z'| \quad (98)$$

This article has been accepted for publication in a future issue of this journal, but has not been fully edited. Content may change prior to final publication. Citation information: DOI 10.1109/ACCESS.2021.3083743, IEEE Access

then the analytical formulas for W_1-W_5 can be obtained. We write

$$W_3(\rho', z') = \int_{-\infty}^{\infty} e^{-u\tau^2} e^{q\tau} d\tau = \sqrt{\pi} e^{\frac{q^2}{4u}} u^{-\frac{1}{2}} \tag{99}$$

$$W_2(\rho', z') = -\frac{dW_3}{du} = \frac{1}{2}\sqrt{\pi} e^{\frac{q^2}{4u}} \left(u^{-\frac{3}{2}} + \frac{q^2}{2} u^{-\frac{5}{2}} \right) \tag{100}$$

$$\begin{aligned} W_1(\rho', z') &= -\frac{dW_2}{du} \\ &= \frac{1}{4}\sqrt{\pi} e^{\frac{q^2}{4u}} \left(3u^{-\frac{5}{2}} + 3q^2 u^{-\frac{7}{2}} + \frac{q^4}{4} u^{-\frac{9}{2}} \right) \end{aligned} \tag{101}$$

$$W_5(\rho', z') = \frac{dW_3}{dq} = \frac{\sqrt{\pi}}{2} q e^{\frac{q^2}{4u}} u^{-\frac{3}{2}} \tag{102}$$

$$W_4(\rho', z') = -\frac{dW_5}{du} = \frac{\sqrt{\pi}}{2} q e^{\frac{q^2}{4u}} \left(\frac{3}{2} u^{-\frac{5}{2}} + \frac{q^2}{4} u^{-\frac{7}{2}} \right) \tag{103}$$

Therefore, the final expressions for (83)-(85) are as following:

$$\begin{aligned} \int_\Gamma f_x^{(1)}(\lambda') H_0^{(1)}(\lambda'\rho') \lambda' d\lambda' = & \frac{2i\varepsilon_3^{\frac{3}{2}} \sqrt{\gamma} e^{ib\rho'}}{\sqrt{\pi\rho'\varepsilon_1}(\varepsilon_1 - \varepsilon_3)(b^2 - a^2)} \\ & \cdot [c_{x1} W_2(\rho', z') + c_{x2} W_3(\rho', z')] \end{aligned} \tag{104}$$

$$\begin{aligned} \int_\Gamma f_x^{(2)}(\lambda') H_1^{(1)}(\lambda'\rho') \lambda' d\lambda' = & \frac{2\varepsilon_3^{\frac{3}{2}} \sqrt{\gamma} e^{ib\rho'}}{\sqrt{\pi\rho'\varepsilon_1}(\varepsilon_1 - \varepsilon_3)(b^2 - a^2)} \\ & \cdot [c_{x3} W_4(\rho', z') + c_{x4} W_5(\rho', z')] \end{aligned} \tag{105}$$

$$\begin{aligned} \int_\Gamma f_x^{(3)}(\lambda') H_2^{(1)}(\lambda'\rho') \lambda' d\lambda' = & \frac{-2i\varepsilon_3^{\frac{3}{2}} \sqrt{\gamma} e^{ib\rho'}}{\sqrt{\pi\rho'\varepsilon_1}(\varepsilon_1 - \varepsilon_3)(b^2 - a^2)} \\ & \cdot [c_{x5} W_2(\rho', z') + c_{x6} W_3(\rho', z')] \end{aligned} \tag{106}$$

By now, we have given the complete procedures for evaluating the near-field of an arbitrarily oriented electric dipole in a magnetized plasma. The formula contains the contributions of both the O-wave and E-wave, where the integral for the O-wave can be directly estimated through numerical integration, while the integral for the E-wave includes a speed-up converged integral and an analytical part. By summing the integrals for both the O-wave and E-wave, the field in the near zone is determined. It is worth mentioning that as the strength of the geomagnetic field B_0 tends to zero, the ionospheric plasma will reduce to an isotropic medium and there is no longer any so-called O-wave or E-wave but only one mode in the isotropic case. This isotropic radiation-field problem can be readily solved with existing techniques in literature.

Moreover, the near-field components E_y, E_z excited by an arbitrary oriented dipole can also be obtained with similar procedures. Detailed formulations for deriving E_y, E_z are provided in Appendix and will not be discussed here. Finally, the field components in cylindrical coordinates are readily obtained via coordinate transformation. We write

$$\begin{bmatrix} E_\rho \\ E_\varphi \\ E_z \end{bmatrix} = \begin{bmatrix} \cos\varphi & \sin\varphi & 0 \\ -\sin\varphi & \cos\varphi & 0 \\ 0 & 0 & 1 \end{bmatrix} \begin{bmatrix} E_x \\ E_y \\ E_z \end{bmatrix} \tag{107}$$

III. COMPUTATIONS AND DISCUSSIONS

Based on the proposed method, we will carry out corresponding computations under several different conditions. The parameters used in computation are selected as follows: the operating frequency is taken as $f = 10$ kHz, the strength of the earth's magnetic field is $B_0 = 0.5 \times 10^{-4}$ T, and the electron density and collision frequency of the ionosphere are taken as $N = 1.4 \times 10^{12}$ m^{-3}, $\nu = 1000$ s^{-1}, then we have $\omega_p = 6.6 \times 10^7$ arc/s, $\omega_c = 8.6 \times 10^6$ arc/s, and the condition $\omega < \omega_c < \omega_p$ is satisfied.

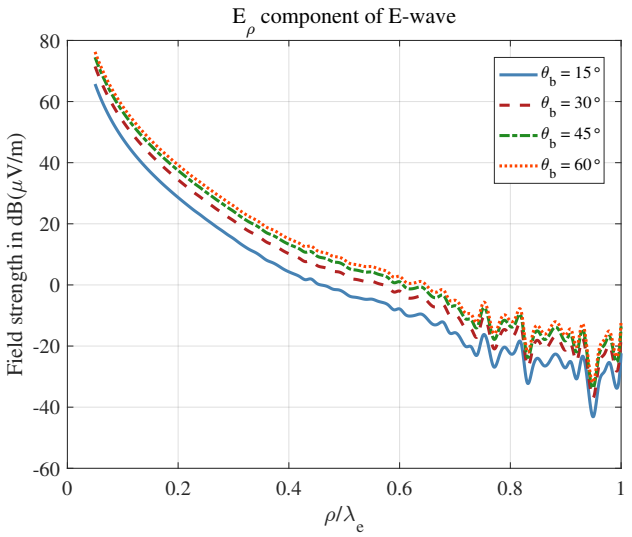

FIGURE 6: Field strength of E_ρ for the E-wave varying with the propagation distance ρ under different geomagnetic dip angles. ($f = 10$ kHz, $z = 0.2\lambda_e$, $\varphi = 0°$.)

Under anisotropic conditions, the field excited by an electric dipole consists of both the O-wave and the E-wave. To investigate the effect of dipole orientation on the field properties of the O-wave and E-wave, the E_ρ component for the E-wave and O-wave versus propagation distance ρ are displayed separately in Figs. 6 and 7 with different geomagnetic tilt angles. The longitudinal propagation distance and azimuth angle are set as $z = 0.2\lambda_e$, $\varphi = 0°$. It is seen that the field strength of both waves decreases with the propagation distance, where the O-wave decays obviously faster than the E-wave. Despite the O-wave is an evanescent wave with large attenuation rate, it still has comparable amplitudes with the E-wave in the near zone (e.g. $\rho < \lambda_e$, $z < \lambda_e$). Therefore, the influence of the O-wave to the total field should never be neglected if we want to calculate the near-field accurately for an anisotropic case. It is worth mentioning that the minima on the O-wave's curves are caused by the phase mutation of the O-wave during propagation and the

This article has been accepted for publication in a future issue of this journal, but has not been fully edited. Content may change prior to final publication. Citation information: DOI 10.1109/ACCESS.2021.3083743, IEEE Access

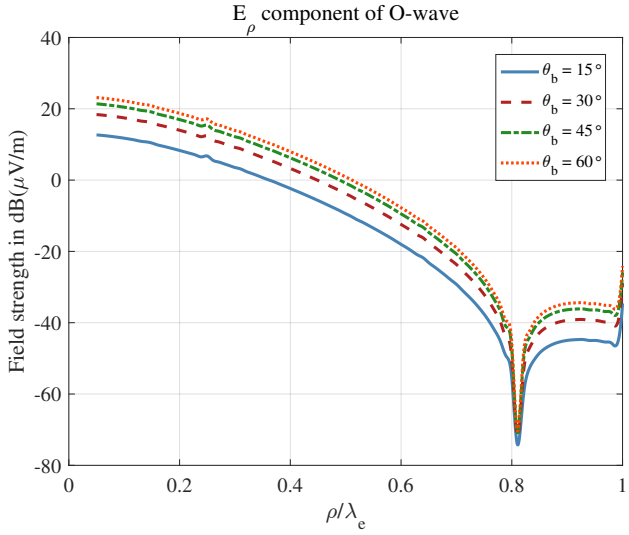

FIGURE 7: Field strength of E_ρ for the O-wave varying with the propagation distance ρ under different geomagnetic dip angles. ($f = 10$ kHz, $z = 0.2\lambda_e$, $\varphi = 0°$.)

locations of those minima exactly coincide with the phase mutation points [19]. Moreover, it is found that the magnitude of both waves increases when the dip angle becomes larger. Since the field excited by an arbitrarily oriented dipole is the superposition of the field due to a vertical electric dipole and a horizontal electric dipole relative to the magnetic field, this phenomenon indicates that the field produced by the horizontal dipole is much stronger than that by the vertical one. We may thus infer that for an arbitrarily oriented electric dipole in a magnetized plasma, the field generated by the dipole perpendicular to the magnetic field is of dominant effects.

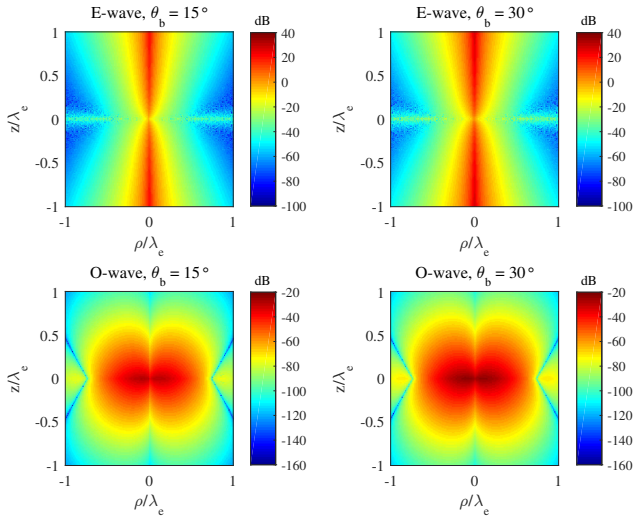

FIGURE 8: Radiation patterns of the E-wave and O-wave at different geomagnetic dip angles. ($f = 10$ kHz, $\theta_b = 15°$ and $30°$, field component: E_z in dB(μV/m).)

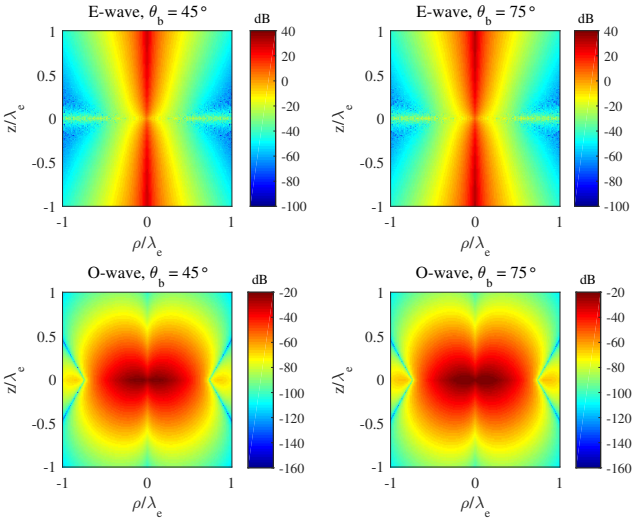

FIGURE 9: Radiation patterns of the E-wave and O-wave at different geomagnetic dip angles. ($f = 10$ kHz, $\theta_b = 45°$ and $75°$, field component: E_z in dB(μV/m).)

To see the field distribution more intuitively, the radiation pattern (in dB(μV/m)) of the E_z component of the dipole is visualized at different dip angles shown in Figs. 8 and 9. It is observed that the field distribution of the O-wave is very similar to that in an isotropic medium, and the larger the dip angle, the more evident the pattern of the O-wave is alike that of a horizontal dipole in free space. However, the radiation pattern of the E-wave exhibits conspicuous "aggregation effect" on the direction of the geomagnetic field, indicating that the propagable mode under an anisotropic condition propagates mainly along the magnetic field. The reason for this fact is that, the attenuation rate of the E-wave will increase with the geomagnetic inclination angle in the VLF range, and the wave will decay faster when the propagation direction deviates from $\theta_b = 0°$. By comparison of the radiation patterns at different angles, it is readily seen that the overall amplitude of the field becomes larger as the dip angle increases, especially when $\theta_b < 45°$. This phenomenon is totally consistent with the one found in Figs. 6 and 7, which is attributed to the dominant field contribution coming from the horizontal electric dipole. Therefore, in order to obtain a stronger radiation field with limited power, the orientation of the dipole should be as perpendicular as possible to the geomagnetic field when placed in the magnetized plasma.

IV. CONCLUSION

We investigate the VLF near-field due to an electric dipole at arbitrary orientation to the magnetic field in a magnetized plasma. The arbitrarily oriented electric dipole is regarded as the superposition of dipoles parallel and perpendicular to the magnetic field. The excited field in this case consists of the contributions of both the O-wave and E-wave, where the O-wave can be directly estimated through numerical integration, and the E-wave in the near zone is evaluated using a speed-up convergence algorithm and the complex

This article has been accepted for publication in a future issue of this journal, but has not been fully edited. Content may change prior to final publication. Citation information: DOI 10.1109/ACCESS.2021.3083743, IEEE Access

variable theory. It is noted that deforming the integration path into the complex plane of λ' may also provide similar effects in improving the convergence of the E-wave's integrands [28]. Computations show that the field strength of the O-wave still has comparable magnitude with the E-wave when the propagation distance is small, and the dipole perpendicular to the magnetic field dominates the near-field. Moreover, the radiation pattern shows that there exists remarkable "aggregation effect" in the field distribution of the E-wave, which implies that the propagable mode in a magnetized plasma mainly orients along the geomagnetic field. By precisely evaluating the near-field of an arbitrarily oriented radiator under anisotropic conditions, this work paves the way for the antenna analysis in realistic VLF space-borne transmitting applications.

APPENDIX. EVALUATION OF THE FIELD COMPONENTS E_Y, E_Z

The near-field components E_y, E_z excited by an arbitrarily oriented electric dipole in a magnetized plasma can also be expressed with the integral contributions from both the O-wave and E-wave. We write

$$E_y(\rho',\varphi,z')=\pm\frac{k_0^2\eta}{4\pi\varepsilon_3}[I_{y1}(\rho',\varphi,z')-I_{y2}(\rho',\varphi,z')] \quad (108)$$

$$E_z(\rho',\varphi,z')=\pm\frac{k_0^2\eta}{4\pi\varepsilon_3}[I_{z1}(\rho',\varphi,z')-I_{z2}(\rho',\varphi,z')] \quad (109)$$

where

$$I_{ym}(\rho',\varphi,z') = -\sin\theta_b I_{ym}^{(1)}(\rho',z') - i\cos\theta_b I_{ym}^{(2)}(\rho',\varphi,z') + \frac{1}{2}\sin\theta_b I_{yj}^{(3)}(\rho',\varphi,z') \quad (110)$$

$$I_{zm}(\rho',\varphi,z') = \cos\theta_b I_{zm}^{(1)}(\rho',z') - i\sin\theta_b I_{zm}^{(2)}(\rho',\varphi,z') \quad (111)$$

and

$$I_{ym}^{(1)}(\rho',z') = \int_0^\infty \frac{p_5'(\lambda')\exp(ik_m'|z'|)}{k_m'(k_1'^2-k_2'^2)}J_0(\lambda'\rho')\lambda' d\lambda' \quad (112)$$

$$I_{ym}^{(2)}(\rho',\varphi,z') = \int_0^\infty \frac{[p_1'(k_m',\lambda')\sin\varphi + p_2'(k_m',\lambda')\cos\varphi]}{k_m'(k_1'^2-k_2'^2)} \cdot \exp(ik_m'|z'|)J_1(\lambda'\rho')\lambda' d\lambda' \quad (113)$$

$$I_{ym}^{(3)}(\rho',\varphi,z') = \int_0^\infty \frac{p_4'(k_m',\lambda')\sin 2\varphi\exp(ik_m'|z'|)}{k_m'(k_1'^2-k_2'^2)} \cdot J_2(\lambda'\rho')\lambda' d\lambda' \quad (114)$$

$$I_{zm}^{(1)}(\rho',z') = \int_0^\infty \frac{p_6'(k_m',\lambda')\exp(ik_m'|z'|)}{k_m'(k_1'^2-k_2'^2)}J_0(\lambda'\rho')\lambda' d\lambda' \quad (115)$$

$$I_{zm}^{(2)}(\rho',\varphi,z') = \int_0^\infty \frac{[p_1'(k_m',\lambda')\cos\varphi + p_2'(k_m',\lambda')\sin\varphi]}{k_m'(k_1'^2-k_2'^2)} \cdot \exp(ik_m'|z'|)J_1(\lambda'\rho')\lambda' d\lambda' \quad (116)$$

In (110)-(116), $m=1$ corresponds to the integrals for the E-wave and $m=2$ corresponds to the integrals for the O-wave. Note that I_{y2} and I_{z2} are also fast converging integrals due to the large imaginary part of k_2', they can be directly evaluated via numerical integration. For the integrals I_{y1} and I_{z1}, the speed-up convergence algorithm is also applied and the resulting formulas are

$$I_{y1}^{(1)}(\rho',z') = \int_0^\infty \left[\frac{p_5'(\lambda')\exp(ik_1'|z'|)}{k_1'(k_1'^2-k_2'^2)} - f_y^{(1)}(\lambda')\right] \cdot J_0(\lambda'\rho')\lambda' d\lambda' + \frac{1}{2}\int_{-\infty}^\infty f_y^{(1)}(\lambda')H_0^{(1)}(\lambda'\rho')\lambda' d\lambda' \quad (117)$$

$$I_{y1}^{(2)}(\rho',\varphi,z') = \int_0^\infty \left\{\frac{[p_1'(k_1',\lambda')\sin\varphi + p_2'(k_1',\lambda')\cos\varphi]\exp(ik_1'|z'|)}{k_1'(k_1'^2-k_2'^2)} - f_y^{(2)}(\lambda')\right\}J_1(\lambda'\rho')\lambda' d\lambda' + \frac{1}{2}\int_{-\infty}^\infty f_y^{(2)}(\lambda')H_1^{(1)}(\lambda'\rho')\lambda' d\lambda' \quad (118)$$

$$I_{y1}^{(3)}(\rho',\varphi,z') = \int_0^\infty \left[\frac{p_4'(k_1',\lambda')\sin 2\varphi\exp(ik_1'|z'|)}{k_1'(k_1'^2-k_2'^2)} - f_y^{(3)}(\lambda')\right]J_2(\lambda'\rho')\lambda' d\lambda' + \frac{1}{2}\int_{-\infty}^\infty f_y^{(3)}(\lambda')H_2^{(1)}(\lambda'\rho')\lambda' d\lambda' \quad (119)$$

$$I_{z1}^{(1)}(\rho',z') = \int_0^\infty \left[\frac{p_6'(k_1',\lambda')\exp(ik_1'|z'|)}{k_1'(k_1'^2-k_2'^2)} - f_z^{(1)}(\lambda')\right] \cdot J_0(\lambda'\rho')\lambda' d\lambda' + \frac{1}{2}\int_{-\infty}^\infty f_z^{(1)}(\lambda')H_0^{(1)}(\lambda'\rho')\lambda' d\lambda' \quad (120)$$

$$I_{z1}^{(2)}(\rho',\varphi,z') = \int_0^\infty \left\{\frac{[p_1'(k_1',\lambda')\cos\varphi + p_2'(k_1',\lambda')\sin\varphi]\exp(ik_1'|z'|)}{k_1'(k_1'^2-k_2'^2)} - f_z^{(2)}(\lambda')\right\}J_1(\lambda'\rho')\lambda' d\lambda' + \frac{1}{2}\int_{-\infty}^\infty f_z^{(2)}(\lambda')H_1^{(1)}(\lambda'\rho')\lambda' d\lambda' \quad (121)$$

where

$$f_y^{(1)}(\lambda') = \frac{p_5'(\lambda')\exp(ik_1^*|z'|)}{k_1^*\sqrt{Q(\lambda')}} \quad (122)$$

$$f_y^{(2)}(\lambda') = \frac{[p_1'(k_1^*,\lambda')\sin\varphi + p_2'(k_1^*,\lambda')\cos\varphi]\exp(ik_1^*|z'|)}{k_1^*\sqrt{Q(\lambda')}} \quad (123)$$

$$f_y^{(3)}(\lambda') = \frac{p_4'(k_1^*,\lambda')\sin 2\varphi\exp(ik_1^*|z'|)}{k_1^*\sqrt{Q(\lambda')}} \quad (124)$$

$$f_z^{(1)}(\lambda') = \frac{p_6'(k_1^*,\lambda')\exp(ik_1^*|z'|)}{k_1^*\sqrt{Q(\lambda')}} \quad (125)$$

$$f_z^{(2)}(\lambda') = \frac{[p_1'(k_1^*,\lambda')\cos\varphi + p_2'(k_1^*,\lambda')\sin\varphi]\exp(ik_1^*|z'|)}{k_1^*\sqrt{Q(\lambda')}} \quad (126)$$

This article has been accepted for publication in a future issue of this journal, but has not been fully edited. Content may change prior to final publication. Citation information: DOI 10.1109/ACCESS.2021.3083743, IEEE Access

With the help of the complex variable theory, the second terms of (117)-(121) can be further expressed as a sum of the residue at the pole and the integral along the branch line. They are

$$\int_{-\infty}^{\infty} f_y^{(1)}(\lambda')H_0^{(1)}(\lambda'\rho')\lambda' d\lambda' = \pi i H_0^{(1)}(a\rho') \cdot \frac{p_5'(a)\exp[ik_1^*(a)|z'|]}{k_1^*(a)\left(1-\frac{\varepsilon_1}{\varepsilon_3}\right)} + \int_{\Gamma} f_y^{(1)}(\lambda')H_0^{(1)}(\lambda'\rho')\lambda' d\lambda' \tag{127}$$

$$\int_{-\infty}^{\infty} f_y^{(2)}(\lambda')H_1^{(1)}(\lambda'\rho')\lambda' d\lambda' = \pi i H_1^{(1)}(a\rho') \cdot \frac{\{p_1'[k_1^*(a),a]\sin\varphi + p_2'[k_1^*(a),a]\cos\varphi\}\exp[ik_1^*(a)|z'|]}{k_1^*(a)\left(1-\frac{\varepsilon_1}{\varepsilon_3}\right)} + \int_{\Gamma} f_y^{(2)}(\lambda')H_1^{(1)}(\lambda'\rho')\lambda' d\lambda' \tag{128}$$

$$\int_{-\infty}^{\infty} f_y^{(3)}(\lambda')H_2^{(1)}(\lambda'\rho')\lambda' d\lambda' = \pi i H_2^{(1)}(a\rho') \cdot \frac{p_4'[k_1^*(a),a]\sin 2\varphi\exp[ik_1^*(a)|z'|]}{k_1^*(a)\left(1-\frac{\varepsilon_1}{\varepsilon_3}\right)} + \int_{\Gamma} f_y^{(3)}(\lambda')H_2^{(1)}(\lambda'\rho')\lambda' d\lambda' \tag{129}$$

$$\int_{-\infty}^{\infty} f_z^{(1)}(\lambda')H_0^{(1)}(\lambda'\rho')\lambda' d\lambda' = \pi i H_0^{(1)}(a\rho') \cdot \frac{p_6'[k_1^*(a),a]\exp[ik_1^*(a)|z'|]}{k_1^*(a)\left(1-\frac{\varepsilon_1}{\varepsilon_3}\right)} + \int_{\Gamma} f_z^{(1)}(\lambda')H_0^{(1)}(\lambda'\rho')\lambda' d\lambda' \tag{130}$$

$$\int_{-\infty}^{\infty} f_z^{(2)}(\lambda')H_1^{(1)}(\lambda'\rho')\lambda' d\lambda' = \pi i H_1^{(1)}(a\rho') \cdot \frac{\{p_1'[k_1^*(a),a]\cos\varphi + p_2'[k_1^*(a),a]\sin\varphi\}\exp[ik_1^*(a)|z'|]}{k_1^*(a)\left(1-\frac{\varepsilon_1}{\varepsilon_3}\right)} + \int_{\Gamma} f_z^{(2)}(\lambda')H_1^{(1)}(\lambda'\rho')\lambda' d\lambda' \tag{131}$$

The latter terms of (127)-(131) represent the integral along the branch line Γ, by using the integral equation of exponential functions, their final analytical forms are given as:

$$\int_{\Gamma} f_y^{(1)}(\lambda')H_0^{(1)}(\lambda'\rho')\lambda' d\lambda' = \frac{2i\varepsilon_3^{\frac{3}{2}}\sqrt{\gamma}e^{ib\rho'}}{\sqrt{\pi\rho'\varepsilon_1}(\varepsilon_1-\varepsilon_3)(b^2-a^2)} \cdot c_{y1}W_3(\rho',z') \tag{132}$$

$$\int_{\Gamma} f_y^{(2)}(\lambda')H_1^{(1)}(\lambda'\rho')\lambda' d\lambda' = \frac{2\varepsilon_3^{\frac{3}{2}}\sqrt{\gamma}e^{ib\rho'}}{\sqrt{\pi\rho'\varepsilon_1}(\varepsilon_1-\varepsilon_3)(b^2-a^2)} \cdot [c_{y2}W_4(\rho',z') + c_{y3}W_5(\rho',z')] \tag{133}$$

$$\int_{\Gamma} f_y^{(3)}(\lambda')H_2^{(1)}(\lambda'\rho')\lambda' d\lambda' = \frac{-2i\varepsilon_3^{\frac{3}{2}}\sqrt{\gamma}e^{ib\rho'}}{\sqrt{\pi\rho'\varepsilon_1}(\varepsilon_1-\varepsilon_3)(b^2-a^2)} \cdot [c_{y4}W_2(\rho',z') + c_{y5}W_3(\rho',z')] \tag{134}$$

$$\int_{\Gamma} f_z^{(1)}(\lambda')H_0^{(1)}(\lambda'\rho')\lambda' d\lambda' = \frac{2i\varepsilon_3^{\frac{3}{2}}\sqrt{\gamma}e^{ib\rho'}}{\sqrt{\pi\rho'\varepsilon_1}(\varepsilon_1-\varepsilon_3)(b^2-a^2)} \cdot [c_{z1}W_1(\rho',z') + c_{z2}W_2(\rho',z') + c_{z3}W_3(\rho',z')] \tag{135}$$

$$\int_{\Gamma} f_z^{(2)}(\lambda')H_1^{(1)}(\lambda'\rho')\lambda' d\lambda' = \frac{2\varepsilon_3^{\frac{3}{2}}\sqrt{\gamma}e^{ib\rho'}}{\sqrt{\pi\rho'\varepsilon_1}(\varepsilon_1-\varepsilon_3)(b^2-a^2)} \cdot [c_{z4}W_4(\rho',z') + c_{z5}W_5(\rho',z')] \tag{136}$$

where

$$c_{y1} = i\varepsilon_2(\varepsilon_3+b^2), \quad c_{y2} = \left(\frac{-2i\gamma b\varepsilon_1}{\varepsilon_3}\right)^{\frac{3}{2}} b\sin\varphi \tag{137}$$

$$c_{y3} = \sqrt{\frac{-2i\gamma b\varepsilon_1}{\varepsilon_3}}b[(b^2-\varepsilon_1)\sin\varphi + i\varepsilon_2\cos\varphi] \tag{138}$$

$$c_{y4} = -\frac{2i\gamma b^3\varepsilon_1}{\varepsilon_3}\sin 2\varphi, \quad c_{y5} = b^2(b^2-\varepsilon_3)\sin 2\varphi \tag{139}$$

$$c_{z1} = -\frac{4\gamma^2 b^2\varepsilon_1^2}{\varepsilon_3^2}, \quad c_{z2} = \frac{4i\gamma b\varepsilon_1^2}{\varepsilon_3} - \frac{2i\gamma b^3\varepsilon_1}{\varepsilon_3} \tag{140}$$

$$c_{z3} = \varepsilon_1^2 - \varepsilon_2^2 - \varepsilon_1 b^2, \; c_{z4} = \left(\frac{-2i\gamma b\varepsilon_1}{\varepsilon_3}\right)^{\frac{3}{2}} b\cos\varphi \tag{141}$$

$$c_{z5} = \sqrt{\frac{-2i\gamma b\varepsilon_1}{\varepsilon_3}}b[(b^2-\varepsilon_1)\cos\varphi + i\varepsilon_2\sin\varphi] \tag{142}$$

After evaluating the integrals of each field component for both the O-wave and E-wave and using (108), (109), the near-field components E_y, E_z are obtained accordingly.

REFERENCES

[1] J. Galejs, Antennas in Inhomogeneous Media. New York, USA: Pergamon Press Inc., 1969.
[2] R. W. P. King et al., Antennas in Matter – Fundamentals, Theory, and Applications. Cambridge, MA, USA: MIT Press, 1981.
[3] R. W. P. King, G. J. Fikioris, and R. B. Mack, Cylindrical Antennas and Arrays. Cambridge, U.K.: Cambridge Univ. Press, 2002.
[4] C. A. Balanis, Antenna Theory – Analysis and Design, 3rd ed. Hoboken, NJ, USA: Wiley, 2005.
[5] R. A. Helliwell, Whistlers and Related Ionospheric Phenomena, 2nd ed. Mineola, NY, USA: Dover, 2006, pp. 23–24.
[6] TSS. NASA Science Missions. Accessed: Mar. 10, 2021. [Online]. Available: http://science.nasa.gov/missions/tss/
[7] R. Deloach, J. Diamond, T. Finely, and R. Rhew, "End-mass instrumentation for the first SEDS/Delta II mission," in Proc. 28th AIAA Aerosp. Sci. Meeting, Reno, NV, USA, Jan. 1990, p. 537.

[8] N. A. Armand et al., "Experimental investigation of the VLF radiation of a loop antenna installed on the Mir-Progress-28-Soyuz TM-2 orbital complex in the earth's ionosphere," (in Russian), Radiotekhnika i Elektronika, vol. 33, pp. 2225–2233, Nov. 1988.
[9] V. A. Koshelev and V. M. Melnikov, Large Space Structures Formed by Centrifugal Forces. Taylor & Francis Group, CRC Press, 1998.
[10] B. W. Reinisch et al., "The radio plasma imager investigation on the IMAGE spacecraft," Space Sci. Rev., vol. 91, pp. 319–359, Jan. 2000.
[11] M. Kruijff et al., "Qualification and in-flight demonstration of a European tether deployment system on YES2," Acta Astronautica, vol. 64, no. 9, pp. 882–905, 2009.
[12] M. Scherbarth et al., "AFRL's demonstration and science experiments (DSX) mission," in Solar Physics and Space Weather Instrumentation III, S. Fineschi and J. A. Fennelly, Ed. San Diego, CA, USA: SPIE, 2009.
[13] J. Lichtenberger et al., "Developing a VLF transmitter for LEO satellites: probing of plasmasphere and radiation belts – the POPRAD proposal," in Proc. 32nd URSI GASS, 2017.
[14] X. Shen et al., "The state-of-the-art of the China seismo-electromagnetic satellite mission," Sci. China Technological Sciences, vol. 61, no. 5, pp. 634–642, May 2018.
[15] L. B. Felsen, "On the use of refractive index diagrams for source excited anisotropic regions," J. Res. Nat. Bur. Standards, vol. 69D, no. 2, pp. 155–169, Feb. 1965.
[16] T. N. C. Wang and T. F. Bell, "VLF/ELF radiation patterns of arbitrarily oriented electric and magnetic dipoles in a cold lossless multicomponent magnetoplasma," J. Geophys. Res., vol. 77, no. 7, pp. 1174–1189, Mar. 1972.
[17] H. G. James, "Electromagnetic whistler-mode radiation from a dipole in the ionosphere," Radio Sci., vol. 38, no. 1, pp. 9-1–9-12, Feb. 2003.
[18] T. W. Chevalier, Near-field characteristics of electric dipole antennas in the inner magnetosphere. Ph.D. Thesis of Standford University, Jan. 2008.
[19] T. He, X. W. Zhang, W. Y. Pan, and K. Li, "Near-field of a VLF electric dipole in an anisotropic plasma," IEEE Trans. Antennas Propag., vol. 67, no. 6, pp. 4040–4048, Jun. 2019.
[20] K. Li and W. Y. Pan, "Radiation of an electric dipole in an anisotropic medium," Indian J. Radio Space Phys., vol. 26, pp. 340–345, Dec. 1997.
[21] W. Y. Pan and K. Li, Propagation of SLF/ELF Electromagnetic Waves. Berlin, Germany: Springer-Verlag, 2014.
[22] T. H. Oswald et al., "Various methods of calibration of the STEREO/WAVES antennas," Advances Space Res., vol. 43, pp. 355–364, Feb. 2009.
[23] H. G. James, " A review of the major developments in our understanding of electric antennas in space plasmas," Radio Sci. Bull., no. 336, Mar. 2011.
[24] J. A. Ratcliffe, The Magneto-Ionic Theory and its Applications to the Ionosphere. New York, USA: Cambridge University Press, 1959.
[25] V. L. Ginzburg, The Propagation of Electromagnetic Waves in Plasma. Oxford, UK: Pergamon Press, 1970.
[26] K. Rawer, D. Bilitza, and S. Ramakrishnan, "Goals and status of the international reference ionosphere," Rev. Geophys. Space Phys., vol. 16, no. 2, pp. 177–181, May 1978.
[27] I. S. Gradshteyn and I. M. Ryzhik, Table of Integrals, Series, and Products, 7th ed. Elsevier Inc., Academic Press, 2007.
[28] V. Silva, C. Régis, and A. Q. Howard Jr, "Complex plane integration in the modelling of electromagnetic fields in layered media: part 1. Application to a very large loop," J. Geophys. Eng., vol. 11, no. 1, 015004, Jan. 2014.

TONG HE was born in Hangzhou, Zhejiang, China, on December 23, 1990. He received the B.S. degree in electrical engineering and automation from University of Electronic Science and Technology of China (UESTC), Chengdu, Sichuan, China, in 2013, the M.S. degree in electrical engineering from The University of Michigan-Dearborn, Dearborn, MI, United States, in 2014, and the Ph.D. degree in electromagnetic field and microwave technology from Zhejiang University, Hangzhou, Zhejiang, China, in 2019, respectively. Since July 2019, he has been a Senior Research Specialist with the Research Center for Intelligent Networks, Zhejiang Laboratory, Hangzhou, Zhejiang, China. His current research interests include electromagnetic wave propagation and antenna theory.

HUI RAN ZENG was born in Chongqing, China, on November 20, 1995. She received the B.S. degree in electronic and information engineering from East China University of Science and Technology, Shanghai, China, in 2017. She is currently working toward the Ph.D. degree in electromagnetic field and microwave technology with the College of Information Science and Electronic Engineering, Zhejiang University, Hangzhou, Zhejiang, China. Her current research interests include radio wave propagation and antenna theory.

KAI LI was born in Xiao County, Anhui, China, on February 10, 1968. He received the B.S. degree in physics from Fuyang Normal University, Fuyang, Anhui, China, in 1990, the M.S. degree in radio physics from Xidian University, Xi'an, Shaanxi, China, in 1994, and the Ph.D. degree in astrophysics from Shaanxi Astronomical Observatory, the Chinese Academy of Sciences, Xi'an, Shaanxi, China, in 1998, respectively.

From August 1990 to December 2000, he was on the faculty of the China Research Institute of Radiowave Propagation (CRIRP), Xinxiang, Henan, China. From January 2001 to December 2002, he was a Post-Doctoral Fellow at Information and Communications University (ICU), Daejeon, Republic of Korea. From January 2003 to January 2005, he was a Research Fellow with the School of Electrical and Electric Engineering, Nanyang Technological University (NTU), Singapore. Since January 2005, he has been a Professor with the College of Information Science and Electronic Engineering, Zhejiang University, Hangzhou, China. His current research interests include classic electromagnetic theory and radio wave propagation.

Dr. Li is a Senior Member of the Chinese Institute of Electronics (CIE) and a Member of the Chinese Institute of Space Science (CISS).